Title

Chronic AT1 blockade improves hyperglycemia by decreasing adipocyte inflammation and decreasing hepatic PCK1 and G6PC1 expression in obese rats

Journal

AJP Endocrinology and Metabolism, 321(5)

ISSN

0193-1849

Authors

Rodriguez, Ruben
Lee, Andrew Y
Godoy-Lugo, Jose A
et al.

Publication Date

2021-11-01

DOI

10.1152/ajpendo.00584.2020

Peer reviewed

Am J Physiol Endocrinol Metab 321: E714–E727, 2021.
First published October 18, 2021; doi:10.1152/ajpendo.00584.2020

american physiological society

AMERICAN JOURNAL OF PHYSIOLOGY
ENDOCRINOLOGY AND METABOLISM

RESEARCH ARTICLE

Chronic AT_1 blockade improves hyperglycemia by decreasing adipocyte inflammation and decreasing hepatic PCK1 and G6PC1 expression in obese rats

Ruben Rodriguez,[1] Andrew Y. Lee,[1] Jose A. Godoy-Lugo,[1] Bridget Martinez,[1] Hiroyuki Ohsaki,[2] Daisuke Nakano,[3] David G. Parkes,[4] Akira Nishiyama,[3] José Pablo Vázquez-Medina, and Rudy M. Ortiz[1]

[1]*Department of Molecular & Cellular Biology, University of California, Merced, California;* [2]*Department of Medical Biophysics, Kobe University Graduate School of Health Sciences, Kobe, Japan;* [3]*Department of Pharmacology, Kagawa University Medical School, Kagawa, Japan;* [4]*DGP Scientific Inc., Del Mar, California; and* [5]*Department of Integrative Biology, University of California, Berkeley, California*

Abstract

Inappropriate activation of the renin-angiotensin system decreases glucose uptake in peripheral tissues. Chronic angiotensin receptor type 1 (AT_1) blockade (ARB) increases glucose uptake in skeletal muscle and decreases the abundance of large adipocytes and macrophage infiltration in adipose. However, the contributions of each tissue to the improvement in hyperglycemia in response to AT_1 blockade are not known. Therefore, we determined the static and dynamic responses of soleus muscle, liver, and adipose to an acute glucose challenge following the chronic blockade of AT_1. We measured adipocyte morphology along with TNF-α expression, F4/80- and CD11c-positive cells in adipose and measured insulin receptor (IR) phosphorylation and AKT phosphorylation in soleus muscle, liver, and retroperitoneal fat before (*T0*), 60 (*T60*) and 120 (*T120*) min after an acute glucose challenge in the following groups of male rats: *1*) Long-Evans Tokushima Otsuka (LETO; lean control; *n* = 5/time point), *2*) obese Otsuka Long Evans Tokushima Fatty (OLETF; *n* = 7 or 8/time point), and *3*) OLETF + ARB (ARB; 10 mg olmesartan/kg/day; *n* = 7 or 8/time point). AT_1 blockade decreased adipocyte TNF-α expression and F4/80- and CD11c-positive cells. In retroperitoneal fat at *T60*, IR phosphorylation was 155% greater in ARB than in OLETF. Furthermore, in retroperitoneal fat AT_1 blockade increased glucose transporter-4 (GLUT4) protein expression in ARB compared with OLETF. IR phosphorylation and AKT phosphorylation were not altered in the liver of OLETF, but AT_1 blockade decreased hepatic *Pck1* and *G6pc1* mRNA expressions. Collectively, these results suggest that chronic AT_1 blockade improves obesity-associated hyperglycemia in OLETF rats by improving adipocyte function and by decreasing hepatic glucose production via gluconeogenesis.

NEW & NOTEWORTHY Inappropriate activation of the renin-angiotensin system increases adipocyte inflammation contributing to the impairment in adipocyte function and increases hepatic *Pck1* and *G6pc1* mRNA expression in response to a glucose challenge. Ultimately, these effects may contribute to the development of glucose intolerance.

adiposity; dyslipidemia; gluconeogenesis; macrophage infiltration; renin-angiotensin system

INTRODUCTION

Obesity increases the risk of developing dyslipidemia and type 2 diabetes (T2D) primarily as a result of its detrimental effects on peripheral insulin sensitivity and pancreatic β-cell function (1–3). Insulin resistance develops due to obesity-associated factors such as inflammation, leptin resistance, and adipocyte dysfunction (4–6). Additionally, obesity increases the circulating levels of components of the renin-angiotensin system (RAS) in animal models and humans (7, 8). Elevated levels of angiotensin II (ANG II), the RAS's primary effector, disrupt insulin signaling in insulin-sensitive tissues (9), suggesting that obesity may contribute to hyperglycemia by inappropriately activating the RAS.

Elevated ANG II levels decrease glucose-stimulated insulin secretion (GSIS) in isolated islets from C57BL/6 mice and blocking ANG II signaling using an angiotensin receptor type 1 (AT_1) blocker (ARB) reverses this effect (9). Furthermore, in a rat model of obesity, metabolic syndrome, and T2D, the beneficial effects of AT_1 blockade on GSIS are dependent on the disease state of the organism at the start of the ARB treatment (10, 11). Regardless of its effects on pancreatic function, chronic AT_1 blockade improves glucose homeostasis by decreasing dyslipidemia and the abundance of large adipocytes (both typically associated with insulin resistance) in a rat model of metabolic syndrome (10). Additionally, in other animal models of obesity and metabolic syndrome, RAS inhibition improves the overall metabolic phenotype by decreasing

Correspondence: R. Rodriguez (rrodriguez3@ucmerced.edu).
Submitted 17 November 2020 / Revised 4 October 2021 / Accepted 7 October 2021

Table 1. *Primer sequences used for qRT-PCR*

Primer Name	Sequence (5′–3′)
FOXO1-FW1	CAGCCAGGCACCTCATAACA
FOXO1-RV1	TCAAGCGGTTCATGGCAGAT
PCK1-FW1	GGATGTGGCCAGGATCGAAA
PCK1-RV1	ATACATGGTGCGGCCTTTCA
G6PC-FW1	AACTCCAGCATGTACCGCAA
G6PC-RV1	GGGCTAGGCAGTAGGGGATA
TBP-FW1	TGGGCTTCCCAGCTAAGTTC
TBP-RV1	TGCTGGTGGGTCAACACAAG

visceral fat mass, abundance of large adipocytes, macrophage infiltration, and improving adipocyte function (12–18). Moreover, RAS inhibition increases insulin-dependent glucose uptake in skeletal muscle in rodent models of obesity and T2D (19, 20), decreases the expression of proteins involved in hepatic gluconeogenesis in type 1 diabetic rats (21), and decreases hepatic triglyceride (TG) accumulation and secretion in obese rats (22). However, the mechanisms by which chronic RAS inhibition improves glucose intolerance and subsequent hyperglycemia are not fully elucidated.

In previous studies, the effects of RAS inhibition on insulin signaling in peripheral tissues were evaluated at a single time point or in a single tissue after exogenous insulin challenge (17, 23–25). Although this method is informative, it does not capture the dynamic cellular responses of all contributing tissues following an acute glucose challenge that would provide insights to the mechanisms contributing to improvements in glucose intolerance. Therefore, the objective of this study was to evaluate the static and dynamic responses of soleus muscle, liver, and adipose to an acute glucose challenge following chronic blockade of AT_1. To address this objective, we used the Otsuka Long Evans Tokushima Fatty (OLETF) rat, which is a model of diet-induced obesity, metabolic syndrome, and T2D (26, 27). We tested the hypothesis that AT_1 blockade decreases hyperglycemia after an acute glucose challenge by improving adipocyte function and decreasing the expression of genes involved in hepatic gluconeogenesis.

METHODS

All experimental procedures were reviewed and approved by the institutional animal care and use committees of Kagawa Medical University (Kagawa, Japan) and the University of California, Merced. The present manuscript complements our previous studies using the same animals, in which we assessed the contributions of AT_1 activation to cardiac redox balance and the contributions of AT_1 and tumor necrosis factor-α activation to blood pressure regulation and renal function (28, 29).

Animals

Ten-week-old male, Long-Evans Tokushima Otsuka (LETO; 279 ± 7 g) and OLETF (359 ± 3 g) rats were studied (Japan SLC Inc., Hamamatsu, Japan). Rats were randomly assigned to their study groups based on body mass (BM), so that the mean BM of the OLETF groups were within 5% of each other at the onset of the study. The study groups were *1*) LETO (lean control; n = 15) + vehicle (0.5% carboxymethyl cellulose in water, by oral gavage once daily), *2*) untreated OLETF (n = 23)

Table 2. *Means (± SD) liver mass and fasting plasma levels for glycoalbumin and total cholesterol*

	LETO	OLETF	OLETF + ARB
Sample sizes, *n*	5–8	6–11	7–10
Liver mass, g	10.2 ± 0.6	17.2 ± 1.0#	15.1 ± 1.3#†
Relative liver mass, g/100 g BM	2.7 ± 0.1	3.2 ± 0.1#	3.0 ± 0.1#†
Glycoalbumin, ng/mL	46 ± 10	69 ± 17#	77 ± 16#
Total cholesterol, mg/dL	46 ± 8	60 ± 9#	63 ± 2#

#$P < 0.05$ vs. LETO, †$P < 0.05$ vs. OLETF. ARB, angiotensin receptor type 1 (AT_1) blocker; BM, body mass; LETO, Long-Evans Tokushima Otsuka; OLETF, Otsuka Long-Evans Tokushima Fatty. Cholesterol and for male 15- to 16-wk-old LETO, OLETF and OLETF + ARB rats.

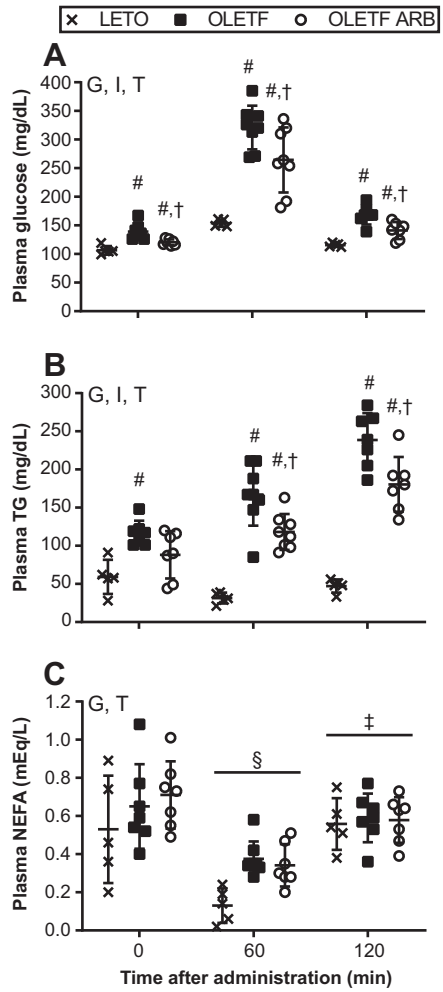

Figure 1. Chronic AT_1 blockade decreases hyperglycemia before and after an acute glucose challenge. Means (±SD) plasma glucose (*A*), TG (*B*), and NEFA (*C*) in Long-Evans Tokushima Otsuka (LETO, n = 5/time point), Otsuka Long-Evans Tokushima Fatty (OLETF, n = 6–8/time point), and OLETF + ARB (n = 6–8/time point) prior (*T0*) and 60 (*T60*) and 120 (*T120*) min after challenge of glucose. Comparisons were assessed using a mixed-model ANOVA with group and time as between-subject factors. Multiple comparisons were carried out using a Holm–Sidak correction. G = group $P < 0.05$; I = interaction $P < 0.05$; T = time $P < 0.05$. #$P < 0.05$ vs. LETO; †$P < 0.05$ vs. OLETF; §$P < 0.05$ vs. *T0*; ‡$P < 0.05$ vs. *T60*. ARB, angiotensin receptor type 1 (AT_1) blocker; NEFA, nonesterified fatty acids; TG, triglyceride.

+ vehicle, and *3*) OLETF + ARB (ARB; 10 mg olmesartan/kg/day by oral gavage at a volume of 500 μL; for 6 wk; n = 22). Olmesartan was chosen because it does not have peroxisome proliferator-activated receptor-γ activity (30), allowing us to better assess the direct effects of AT_1 inhibition on glucose homeostasis independent of PPARγ. All animals were maintained in groups of three or four animals per cage in a specific pathogen-free facility under controlled temperature (23°C) and humidity (55%) with a 12-h light, 12-h dark cycle. All animals were given free access to water and standard laboratory rat chow consisting of 5% fat, 24% protein, and 54% carbohydrates (MF; Oriental Yeast Corp., Tokyo, Japan).

Body Mass

BM was measured every day to calculate the appropriate ARB dose (28, 29) and to confirm the diet-induced obesity phenotype.

Blood Pressure

Systolic blood pressure was measured in conscious rats by tail-cuff plethysmography (BP-98A; Softron Co., Tokyo, Japan) (28, 29) to confirm the strain-dependent hypertension and the effectiveness of the ARB treatment.

Tissue Collection

At the end of the study, animals were randomly assigned to three different subgroups within each group: LETO (n = 5/time point), OLETF (n = 7 or 8/time point), and ARB (n = 7 or 8/time point). Subgroups corresponded to animals that were taken following a 12-h fast at baseline (*T0*) and 60 (*T60*) and 120 (*T120*) min after an acute glucose challenge (2 g/kg) (28). Animals were decapitated, and trunk blood was collected into chilled vials containing 50 mM EDTA and protease inhibitor cocktail (PIC; Sigma-Aldrich, St. Louis, MO). Immediately after, the liver, soleus muscle, and retroperitoneal and epididymal fat depots were rapidly removed, weighed, and snap-frozen in liquid nitrogen. Additionally, a piece of retroperitoneal fat and liver was fixed in 4% paraformaldehyde, dehydrated, and embedded in paraffin. Frozen samples were kept at −80°C until analyzed. Blood samples were centrifuged (3,000 *g* for 15 min at 4°C), and plasma was transferred to cryovials, frozen by immersion in liquid nitrogen, and immediately stored at −80°C.

Histological Analysis of Adipose Tissue and Liver

Paraffin-embedded retroperitoneal fat was sectioned (10 μm thick), deparaffinized, rehydrated, and stained with hematoxylin and eosin (H&E; Sigma-Aldrich, St. Louis, MO). The adipocyte area was measured as previously described (10). Paraffin-embedded liver samples were sectioned (5-μm thick), deparaffinized, rehydrated, and stained with H&E at the UC Davis Research Histology Core. H&E-stained sections of liver were used to quantify lipid deposition using the particle analysis function in Fiji-ImageJ as previously described (31). Hepatic fibrosis and necrosis were evaluated by a pathologist in a blind fashion.

Immunofluorescence

The sections used for histology were deparaffinized, rehydrated using xylene and ethanol, permeabilized, blocked, and incubated overnight at 4°C with primary antibodies (F4/80, GenTex, Cat. No. GTX101895, 1:100 dilution; CD11c, Abcam, Cat. No. ab11029, 1:150 dilution; TNF-α Invitrogen, Cat. No. PA5-19810, 1 μg/mL) as previously described (32). Sections were washed and incubated

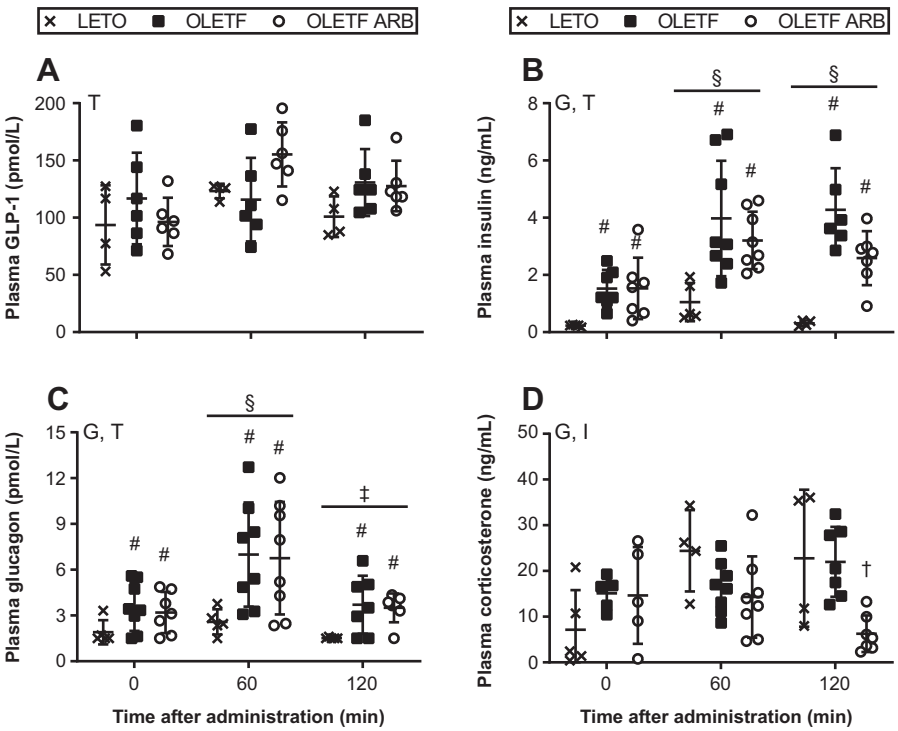

Figure 2. Effects of chronic AT_1 blockade on glucoregulatory hormones. Means (±SD) plasma GLP-1 (*A*), insulin (*B*), glucagon (*C*), and corticosterone (*D*) in Long-Evans Tokushima Otsuka (LETO; n = 4 or 5/time point), Otsuka Long-Evans Tokushima Fatty (OLETF; n = 5–8/time point), and OLETF + ARB (n = 5–8/time point) prior (*T0*) and 60 (*T60*) and 120 (*T120*) min after challenge of glucose. Comparisons were assessed using a mixed-model ANOVA with group and time as between-subject factors. Multiple comparisons were carried out using a Holm–Sidak correction. G = group $P < 0.05$; I = interaction $P < 0.05$; T = time $P < 0.05$. #$P < 0.05$ vs. LETO; †$P < 0.05$ vs. OLETF; §$P < 0.05$ vs. *T0*; ‡$P < 0.05$ vs. *T60*. ARB, angiotensin receptor type 1 (AT_1) blocker; GLP-1, glucagon-like peptide-1.

with Alexa Fluor 488- or 594-specific secondary antibodies diluted 1:200, and with anti-perilipin-Alexa 405-conjugated antibodies diluted 1:100 (Novus, Cat. No. NB110-40760AF405). Sections were mounted using Vectashield antifade mounting medium and imaged at the UC Berkeley Molecular Imaging Center using a Zeiss LSM 780 AxioExaminer microscope fitted with a ×20 water-immersion objective. F4/80- and CD11c-positive cells and adipocytes in six different fields per slide were counted using Fiji-ImageJ. Results are expressed in % of positive cells per 100 adipocytes (33). The signal intensity of TNF-α was quantified from at least seven fields per slide using Fiji-ImageJ. The signal intensity from the seven fields was averaged, and results are presented as change from LETO.

Quantitative PCR

Total RNA was isolated using TRIzol reagent (Invitrogen, Carlsbad, CA). RNA concentration and integrity were analyzed by measuring the absorbance at 260/280 nm and by 1% agarose gel electrophoresis. Contamination of genomic DNA in total RNA was eliminated by digestion with DNase I (Roche, Indianapolis, IN). Total DNA-free RNA (2 μg) was used to synthesize cDNA for each sample using oligo-dT and the high-capacity cDNA reverse transcription kit (Applied Biosystems, Foster City, CA). Specific primers for each gene

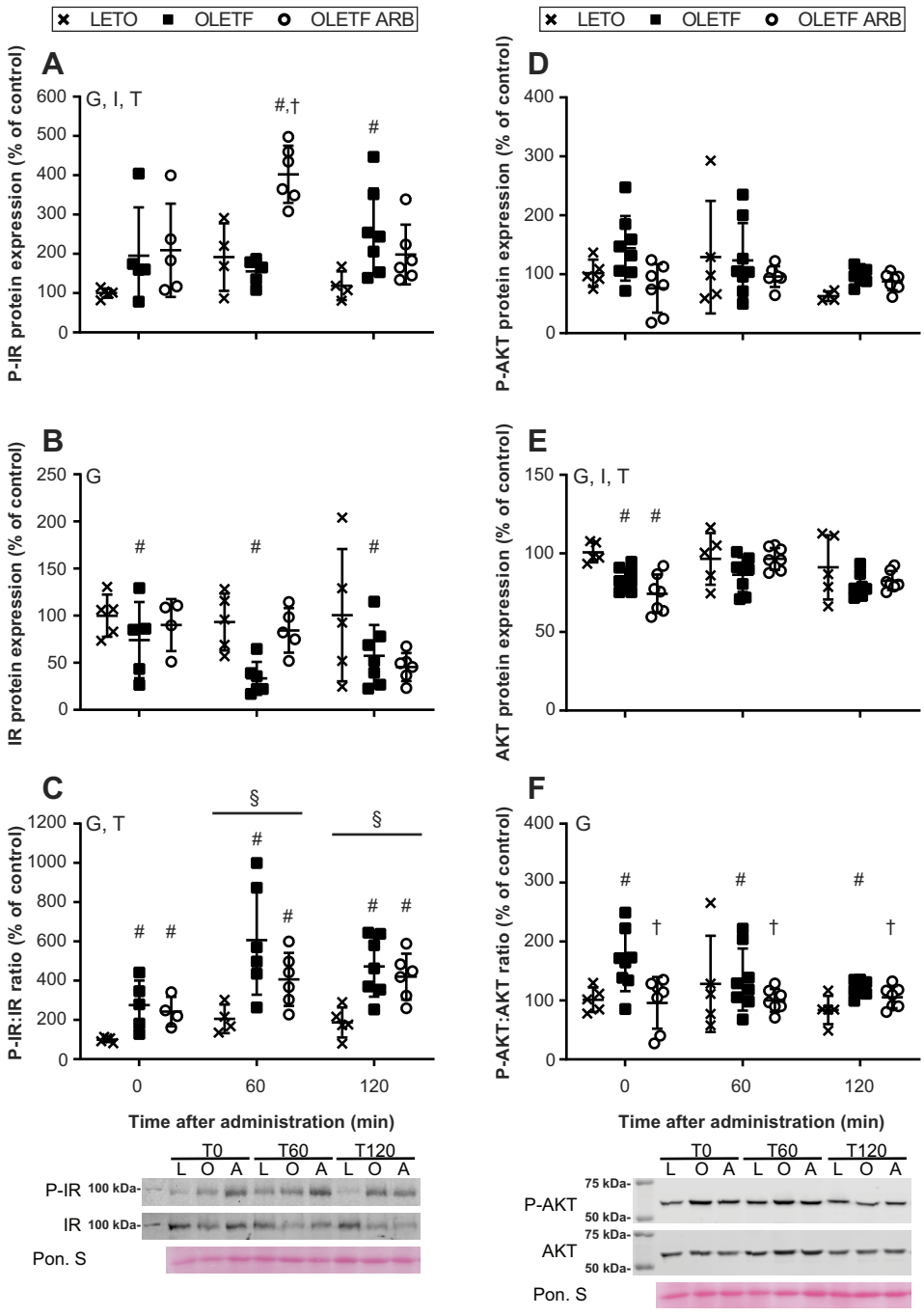

Figure 3. Chronic AT$_1$ blockade increases IR phosphorylation in retroperitoneal fat of Otsuka Long-Evans Tokushima Fatty (OLETF) rats. Means (±SD) IR phosphorylation (*A*), IR-β (*B*), p-IR:IR-β ratio (*C*), AKT phosphorylation (*D*), AKT (*E*), and p-AKT:AKT ratio (*F*) [% change from Long-Evans Tokushima Otsuka (LETO) *T0*] and their representative Western blot bands in LETO (n = 4 or 5/time point), OLETF (n = 5–8/time point), and OLETF + ARB (n = 5–8/time point) prior (*T0*) and 60 (*T60*) and 120 (*T120*) min after challenge of glucose. Comparisons were assessed using a mixed-model ANOVA with group and time as between-subject factors. Multiple comparisons were carried out using a Holm–Sidak correction. G = group $P < 0.05$; I = interaction $P < 0.05$; T = time $P < 0.05$. #$P < 0.05$ vs. LETO; †$P < 0.05$ vs. OLETF; §$P < 0.05$ vs. *T0*. ARB, angiotensin receptor type 1 (AT$_1$) blocker; IR, insulin receptor.

were designed based on the nucleotide sequences deposited in the GenBank database (Table 1). qPCR reactions were performed for Forkhead box protein O1 (*Foxo1*), phosphoenolpyruvate carboxykinase 1 (*Pck1*), and glucose-6-phosphatase 1 (*G6pc1*). PCR reactions were run in duplicate (QuantStudio 3 Real-Time PCR System, Applied Biosystems, Foster City, CA) in a final volume of 15 μL containing 7.5 μL of Power SYBR Green PCR Master Mix (Applied Biosystems, Foster City, CA), 5.5 μL of H_2O, 0.50 μL of each primer (20 μM), and 1 μL of cDNA (equivalent to 100 ng of the original total RNA). After an initial denaturing step at 94°C for 10 min, amplifications were performed for 40 cycles at 94°C for 15 s and 63°C for 1 min with a single fluorescence measurement, and a final melting curve program increasing 0.3°C each 20 s from 60°C to 95°C. Positive and negative controls were included for each gene. Standard curves for each gene were run to determine the efficiency of amplification using dilutions from $5E^{-2}$ to $5E^{-7}$ ng/μL of PCR fragments. Quantitative PCR reactions were performed separately for each gene and normalized by the mRNA expression of TATA box binding protein (*Tbp*).

Western Blot Analyses

For whole cell homogenates, proteins were extracted and assayed as previously described (10). Plasma membrane proteins from the soleus were extracted using a commercially available kit (Invent Biotechnologies, Plymouth MN). Blots were incubated with the following antibodies: phosphorylated (p)-IGF-1 receptor-β (Tyr1135/1136)/(p)-insulin receptor (IR)-β 1:500 (Tyr1150/1151; Cat. No. 3024), p-AKT 1:1,000 (ser473; Cat. No. 4060), AKT 1:2,000 (Cat. No. 4691), GAPDH 1:1,000 (Cat. No. 2118), glucose transporter-4 1:1,000 (GLUT4; Cat. No. 2213, Cell Signaling, Danvers, MA), IR-β 1:500 (Cat. No. SC-711), sodium-potassium ATPase 1:250 (Na^+/K^+ ATPase; Santa Cruz Biotechnology, Santa Cruz, CA), and glucose transporter-4 1:1,000 (GLUT4; Cat. No. ab654, Abcam, Cambridge, MA) in Odyssey blocking solution + 0.2% Tween 20 at 4°C. Membranes were scanned in an Odyssey infrared imager (LI-COR Biosciences, Lincoln, NE) or an Azure c500 imager (Azure Biosystems, Dublin, CA). In addition to loading the same amount of total protein per well, densitometry values were further normalized by correcting for the densitometry values of Ponceau S staining as previously described (28) or total protein stain (LI-COR Biosciences, Lincoln, NE). Western blot results were acquired from a total of four to six blots that were run simultaneously. All Western blots included one to two samples from each group at all three time points. Densitometry values from each protein were divided by the densitometry values of the total protein stain. Results are presented as percent change from LETO at *T0*.

Biochemical Analyses

Fasting plasma glucose, total cholesterol (TC), and TG were measured using an automatic analyzer (7020 clinical analyzers, Hitachi, Tokyo, Japan). Plasma nonesterified fatty acids were measured using a commercially available kit (WAKO, Osaka, Japan). Plasma adiponectin, corticosterone (R&D Systems, Minneapolis, MN), glycated albumin (My BioSource, San Diego, CA), glucagon (Mercodia Inc., Winston Salem, NC), glucagon-like peptide-1 (Phoenix Pharmaceuticals, Inc., Burlingame, CA), and insulin (EMD Millipore, Billerica, MA) were measured using commercially available, rat-specific RIA and ELISA kits. All samples were analyzed in duplicate with intra-assay, percent coefficients of variability of <10% for all assays.

Statistics

Means (± standard deviation) were calculated using all samples unless otherwise noted. We used a one-way ANOVA followed by Tukey's post hoc test for BM, systolic blood pressure (SBP), and organ masses. For all other data, we used a mixed model ANOVA with group and time as between-subject factors unless otherwise specified in the figure legend. When significant differences were observed, multiple comparisons were carried out using a Holm–Sidak correction. Outliers were detected using Grubbs' test and removed. Statistical significance was set at $P < 0.05$. Statistical analyses were performed with GraphPad Prism 8.4.3 (GraphPad Software, San Diego, CA).

RESULTS

AT_1 Blockade Protected against Lean Body Mass Loss and Reduced Fat Accumulation

Mean BM, relative soleus muscle, liver, and epididymal and retroperitoneal fat masses were measured to assess the effects of AT_1 blockade on body composition. Data on BM, SBP, and relative epididymal and retroperitoneal fat masses have been previously published (28, 29) but are briefly

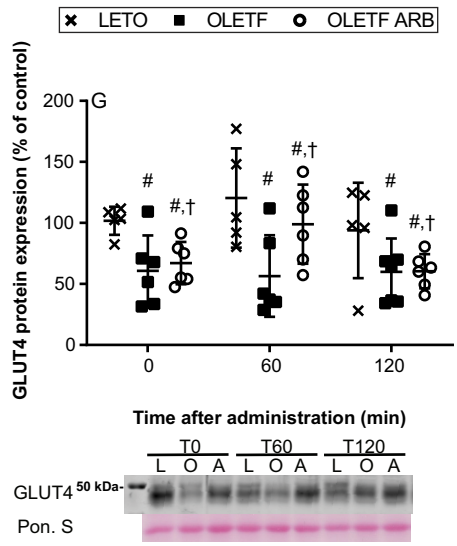

Figure 4. Chronic AT_1 blockade increases retroperitoneal fat GLUT4 protein expression. Means (±SD) GLUT4 protein expression [% change from Long-Evans Tokushima Otsuka (LETO) *T0*] and the representative Western blot bands of LETO (n = 5/time point), Otsuka Long-Evans Tokushima Fatty (OLETF; n = 6–8/time point), and OLETF + ARB (n = 6–8/time point) prior (*T0*) and 60 (*T60*) and 120 (*T120*) min after challenge of glucose. Comparisons were assessed using a mixed-model ANOVA with group and time as between-subject factors. Multiple comparisons were carried out using a Holm–Sidak correction. G = group $P < 0.05$. #$P < 0.05$ vs. LETO; †$P < 0.05$ vs. OLETF. ARB, angiotensin receptor type 1 (AT_1) blocker; GLUT4, glucose transporter-4.

included here for context. At the end of the study, BM was greater in OLETF compared with LETO (366 ± 32 vs. 503 ± 24 g; $P < 0.05$) and ARB (481 ± 11 g; $P > 0.05$) did not affect BM (28, 29). SBP was greater in OLETF compared with LETO (114 ± 6 vs. 142 ± 5 mmHg; $P < 0.05$) and ARB (120 ± 6 mmHg; $P < 0.05$ vs. OLETF) completely reversed the elevated arterial pressure (28, 29). Relative soleus mass was reduced 19% in OLETF compared with LETO (0.042 ± 0.004 vs. 0.034 ± 0.002 g/100 g BM; $P < 0.05$) and ARB (0.037 ± 0.004 g/100 g BM; $P > 0.05$ vs. LETO) prevented this effect. Absolute and relative liver masses were increased 69% and 19%, respectively, in OLETF compared with LETO. ARB decreased absolute and relative liver masses by 12% and 6%, respectively, compared with OLETF (Table 2). Relative epididymal and retroperitoneal fat masses were 83% (1.2 ± 0.1 vs. 2.2 ± 0.3 g/100 g BM; $P < 0.05$) and 170% (1.5 ± 0.1 vs. 4.0 ± 0.6 g/100 g BM; $P < 0.05$) greater, respectively, in OLETF compared with LETO. ARB reduced relative epididymal and retroperitoneal fat masses by 14% (1.9 ± 0.1 g/100 g BM; $P < 0.05$) and 20% (3.2 ± 0.4 g/100 g BM; $P < 0.05$), respectively, compared with OLETF (29). Collectively, these results demonstrated that AT_1 blockade normalizes relative lean body mass and reduces the accumulation of fat in OLETF rats.

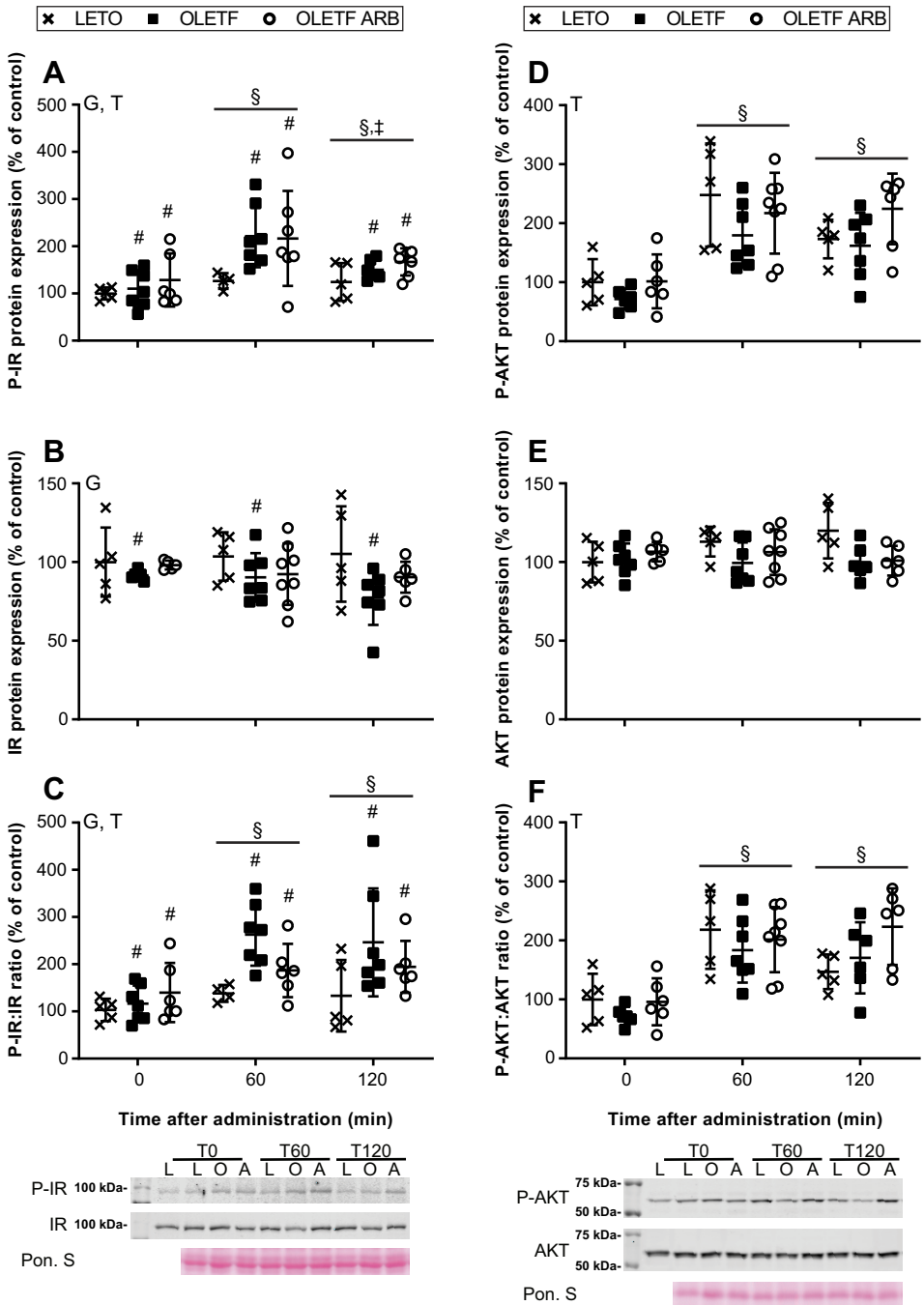

Figure 5. IR phosphorylation and AKT phosphorylation are not impaired in soleus of Otsuka Long-Evans Tokushima Fatty (OLETF) rats. Means (±SD) IR phosphorylation (*A*), IR-β (*B*), p-IR:IR-β ratio (*C*), AKT phosphorylation (*D*), AKT (*E*), and p-AKT:AKT ratio (*F*) [% change from Long-Evans Tokushima Otsuka (LETO) *T0*] and their representative Western blot bands in LETO (n = 4 or 5/time point), OLETF (n = 6–8/time point), and OLETF + ARB (n = 6–8/time point) prior (*T0*) and 60 (*T60*) and 120 (*T120*) min after challenge of glucose. Comparisons were assessed using a mixed-model ANOVA with group and time as between-subject factors. Multiple comparisons were carried out using a Holm–Sidak correction. G = group $P < 0.05$; T = time $P < 0.05$. #$P < 0.05$ vs. LETO; §$P < 0.05$ vs. *T0*; ‡$P < 0.05$ vs. *T60*. ARB, angiotensin receptor type 1 (AT_1) blocker; IR, insulin receptor.

AT_1 Blockade Decreased the Glucose and TG Responses to an Acute Glucose Challenge

Plasma glucose, TG, nonesterified fatty acids (NEFA), glycated albumin, TC, glucagon-like peptide-1 (GLP-1), insulin, glucagon, corticosterone, and adiponectin were measured to assess the responses of chronic AT_1 blockade on lipid and glucoregulatory hormones to an acute glucose challenge. At all-time points, mean plasma glucose was greater in OLETF than in LETO and ARB reduced it (Fig. 1*A*). At *T0*, plasma TG levels were greater in OLETF compared with LETO. At *T60* and *T120*, plasma TG increased in OLETF and ARB compared with LETO, and levels decreased 28% and 38% in ARB at *T60* and *T120*, respectively, compared with OLETF (Fig. 1*B*). There were significant group and time effects on plasma NEFA. Mean plasma NEFA decreased in response to the glucose challenge. Mean plasma NEFA levels were greater in OLETF and ARB than LETO (P = 0.0508; Fig. 1*C*). Baseline mean plasma glycated albumin was 50% and 67% greater in OLETF and ARB, respectively, compared with LETO (Table 2). Additionally, baseline mean plasma TC was 30% and 37% higher in OLETF and ARB, respectively, compared with LETO (Table 2). There was a significant time but no group effect on plasma GLP-1 (Fig. 2*A*). There were significant group and time effects on mean plasma insulin and glucagon. Mean plasma insulin and glucagon increased with the glucose challenge. Furthermore, plasma insulin and glucagon were greater in OLETF and ARB than in LETO (Figs. 2*B* and 1*C*). At *T0* and *T60*, mean plasma corticosterone was not different between the groups; however, at *T120*, mean plasma corticosterone was 72% lower in ARB than OLETF (Fig. 2*D*). There was a significant group but no time effect on plasma adiponectin. Mean group plasma adiponectin was greater in OLETF (4.7 ± 0.8 μg/mL; $P < 0.05$) and ARB (4.5 ± 0.8 μg/mL; $P < 0.05$) compared with LETO (3.7 ± 0.5 μg/mL). These results collectively demonstrated that AT_1 blockade reduces glucose intolerance and that these effects are independent of its effects on glucose regulatory hormones during these measurement periods. These results also demonstrated that AT_1 blockade reduces the typical OLETF TG response to an acute glucose challenge.

Chronic AT_1 Blockade Increased IR Phosphorylation in Retroperitoneal Fat after an Acute Glucose Challenge

IR phosphorylation and AKT phosphorylation were measured in retroperitoneal fat and soleus muscle at baseline (*T0*) and 60 (*T60*) and 120 (*T120*) min after an acute glucose challenge to determine the impacts of the obesity-associated hyperglycemia, and ARB treatment, on peripheral IR phosphorylation and AKT phosphorylation.

Retroperitoneal fat.

At *T0*, mean IR phosphorylation was not different among the groups; however, at *T60*, IR phosphorylation was 155% greater in ARB than in OLETF, and at *T120*, IR phosphorylation was 116% greater in OLETF than in LETO (Fig. 3*A*). There was a significant group but no time effect on IR. Mean IR was lower in OLETF than in LETO, and ARB was not different from LETO or OLETF (Fig. 3*B*). There were significant group and time effects on the ratio of IR phosphorylation and nonphosphorylated IR (p-IR:IR). Mean p-IR:IR ratio was greater in OLETF and ARB compared with LETO (Fig. 3*C*). There was no group or time effect on AKT phosphorylation (Fig. 3*D*). At *T0*, mean AKT was lower in OLETF and ARB than in LETO (Fig. 3*E*). There was a significant group but no time effect on the ratio of AKT phosphorylation and nonphosphorylated AKT (p-AKT:AKT; Fig. 3*F*). Mean p-AKT:AKT ratio was greater in OLETF than in LETO, and ARB normalized the levels (Fig. 3*F*). Additionally, glucose transporter-4 (GLUT4) protein expression was measured in retroperitoneal fat to determine the contribution of AT_1-mediated signaling on GLUT4 protein expression. There was a significant group but no time effect on GLUT4. Mean GLUT4 was lower in OLETF and OLETF + ARB compared with LETO; however, mean GLUT4 was greater in OLETF + ARB than in OLETF (Fig. 4). In summary, these results indicate that acute glucose exposure alters IR phosphorylation and GLUT4 expression in retroperitoneal fat of OLETF rats and that these effects are partially mitigated by ARB treatment.

Soleus muscle.

There were significant group and time effects on soleus IR phosphorylation and p-IR:IR ratio; however, there was only a group effect on IR (Fig. 5, *A*–*C*). Mean IR phosphorylation increased following the acute glucose challenge in all the groups, and the response was greater in OLETF and ARB than in LETO (Fig. 5*A*). Mean p-IR:IR ratio increased

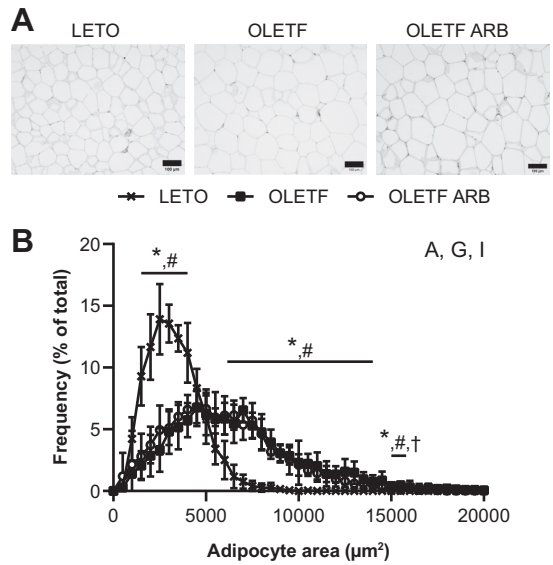

Figure 6. Effects of chronic AT_1 blockade on adipocyte morphology. *A*: representative images of adipocytes from retroperitoneal fat. Means (±SD) adipocyte area distribution (*B*) of Long-Evans Tokushima Otsuka (LETO; n = 5), Otsuka Long-Evans Tokushima Fatty (OLETF; n = 7), and OLETF + ARB (n = 7). Comparisons were assessed using a mixed-model ANOVA with group as between-subjects factor and adipocyte area as a within-subjects factor/multiple comparisons were carried out using a Holm–Sidak correction. A = adipocyte area $P < 0.05$; G = group $P < 0.05$; I = interaction $P < 0.05$. *$P < 0.05$ LETO vs. OLETF; *$P < 0.05$ LETO vs. OLETF + ARB; †$P < 0.05$ OLETF vs. OLETF + ARB. ARB, angiotensin receptor type 1 (AT_1) blocker.

postglucose challenge in all the groups, and it was greater in OLETF and ARB than in LETO (Fig. 5*C*). There was a significant time but no group effect on AKT phosphorylation and p-AKT:AKT ratio. Mean AKT phosphorylation and p-AKT:AKT were greater postglucose challenge in all the groups compared with *T0* (Fig. 5, *D* and *F*). There was no group or time effect on AKT (Fig. 5*E*). We also measured GLUT4 protein expression in the plasma membrane from soleus and found no difference among the groups (data not shown). These results collectively suggest that acute glucose exposure does not alter IR phosphorylation or AKT phosphorylation and GLUT4 translocation in soleus at this stage in OLETF rats.

Chronic AT_1 blockade decreased adipocyte inflammation. Adipocyte morphology, along with TNF-α, and F4/80- and CD11c-positive cells in adipose were measured to assess whether the improvement in IR phosphorylation and GLUT4 expression was associated with a reduction in the relative abundance of large adipocytes and adipocyte inflammation. The abundance of adipocytes between 1,500 and 4,000 μm^2 was greater in OLETF and OLETF + ARB than in LETO (Fig. 6, *A* and *B*). Additionally, the abundance of adipocytes between 6,000 and 14,000 μm^2 was greater in OLETF and OLETF + ARB than in LETO (Fig. 6, *A* and *B*). AT_1 blockade reduced the abundance of adipocytes between 15,000 and 15,500 μm^2 as compared with OLETF (Fig. 6, *A* and *B*). Adipocyte F4/80- and CD11c-positive cells were 173% and 174% greater, respectively, in OLETF compared with LETO, and ARB normalized the levels (Fig. 7, *A–C*). Adipocyte TNF-α levels decreased 52% in OLETF + ARB compared with OLETF (Fig. 8, *A* and *B*). These results collectively demonstrated that prophylactic treatment with Olmesartan in 10-wk-old OLETF rats has modest effects on adipocyte morphology but does help prevent the inflammatory state observed in adipose of untreated OLETF rats.

Chronic AT_1 Blockade Decreased the Expression of Genes Involved in Hepatic Gluconeogenesis

IR phosphorylation and AKT phosphorylation along with *Pck1* and *G6pc1* mRNA expressions were measured in the liver at baseline (*T0*) and 60 (*T60*) and 120 (*T120*) min after an acute glucose challenge to evaluate the contributions of AT_1-mediated signaling on hepatic IR phosphorylation and AKT phosphorylation and gluconeogenesis. There were significant group and time effects on hepatic IR phosphorylation. Mean IR phosphorylation increased in all the groups 60 min postglucose challenge (Fig. 9*A*). Mean IR phosphorylation was greater in OLETF and ARB than in LETO (Fig. 9*A*).

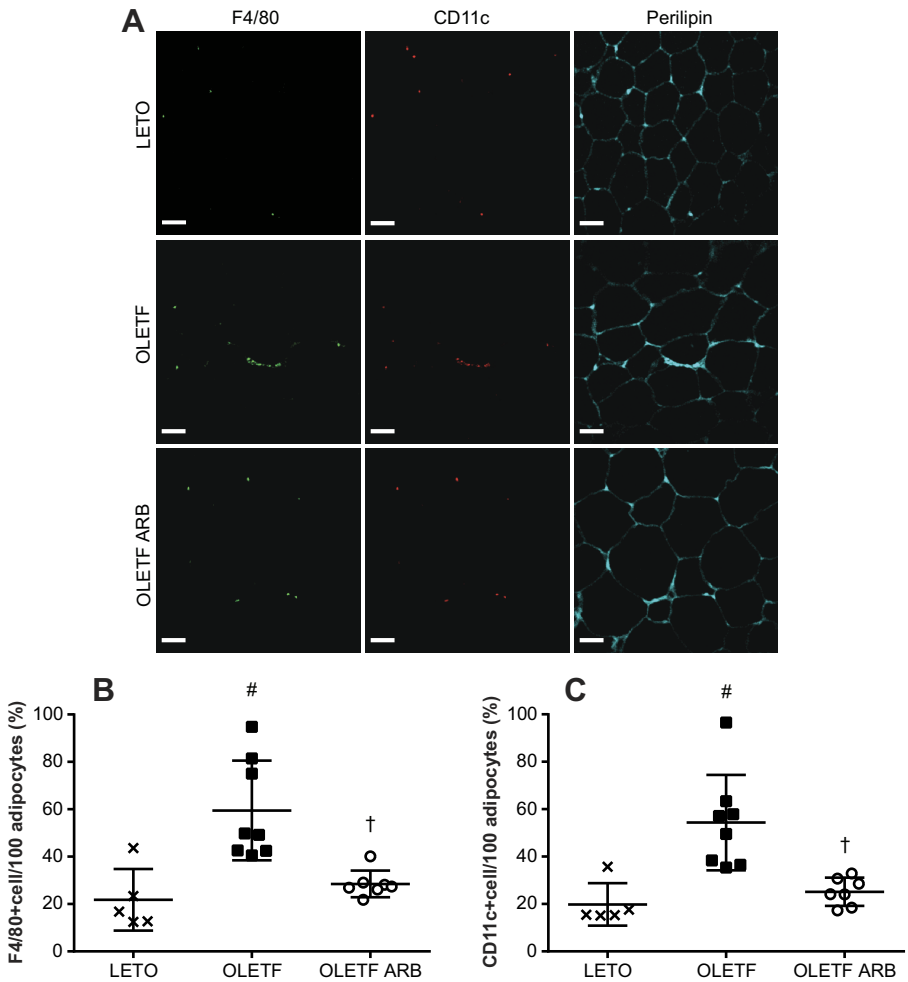

Figure 7. Chronic AT_1 blockade decreases macrophage infiltration in retroperitoneal adipose tissue. *A*: representative images of adipocytes stained with F4/80, CD11c, and perilipin. Means (±SD) $F4/80^+$ (*B*) and (*C*) $CD11c^+$ cells of Long-Evans Tokushima Otsuka (LETO; $n = 5$), Otsuka Long-Evans Tokushima Fatty (OLETF; $n = 8$), and OLETF + ARB ($n = 7$). For $F4/80^+$, comparisons were assessed using a one-way ANOVA followed by Holm–Sidak post hoc test. For $CD11c^+$, comparisons were assessed using a Krustal–Wallis test followed by Dunn's post hoc test. #$P < 0.05$ vs. LETO; †$P < 0.05$ vs. OLETF. ARB, angiotensin receptor type 1 (AT_1) blocker. Scale bar = 100 μm.

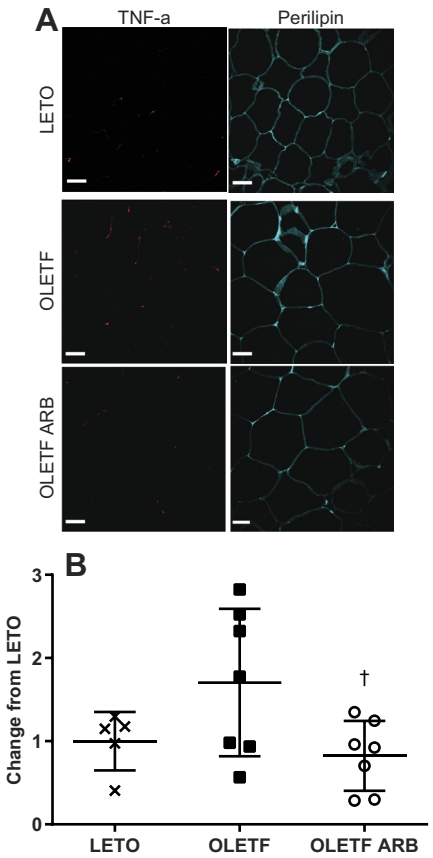

Figure 8. AT_1 blockade reduces adipocyte TNF-α levels. *A*: representative images of adipocytes stained with TNF-α and perilipin. Means (±SD) TNF-α intensity (*B*) of Long-Evans Tokushima Otsuka (LETO; $n = 5$), Otsuka Long-Evans Tokushima Fatty (OLETF; $n = 7$), and OLETF + ARB ($n = 7$). Comparisons were assessed using a one-way ANOVA followed by Tukey's post hoc test. †$P < 0.05$ vs. OLETF. ARB, angiotensin receptor type 1 (AT_1) blocker. Scale bar = 100 μm.

There was a significant group but no time effect on IR. Mean IR was lower in OLETF and ARB compared with LETO (Fig. 9*B*). There was a significant group but no time effect on p-IR:IR ratio. Mean p-IR:IR ratio was greater in OLETF and ARB compared with LETO (Fig. 9*C*). There was a significant time but no group effect on AKT phosphorylation and p-AKT:AKT ratio (Fig. 9, *D* and *F*). There was no group or time effect on AKT (Fig. 9*E*).

mRNA expression.

There was a significant time but no group effect on *Foxo1* mRNA expression (Fig. 10*A*). At *T0* and *T60*, mean *Pck1* mRNA expression was not different between LETO and OLETF; however, at *T0* and *T60*, mean *Pck1* mRNA expressions were reduced by 58% and 64%, respectively, in ARB compared with OLETF (Fig. 10*B*). At *T120*, mean *Pck1* mRNA expression was reduced by 70% and 85% in OLETF and ARB, respectively, compared with LETO (Fig. 10*B*). At *T0* and *T120*, mean *G6pc1* mRNA expressions were not different among the groups (Fig. 10*C*). At *T60*, mean *G6pc1* mRNA expression was 6.0-fold greater in OLETF than in LETO, and ARB normalized the levels (Fig. 10*C*). These results collectively suggest that acute glucose exposure does not alter hepatic IR phosphorylation and AKT phosphorylation at this stage of the disease in OLETF rats. However, AT_1-mediated signaling is sufficiently elevated to contribute to the hyperglycemia such that chronic blockade of AT_1 decreases the potential for de novo hepatic glucose production.

Hepatic injury.

Additionally, hepatic lipid deposition, fibrosis, and necrosis were evaluated to determine whether the improvements in gluconeogenic enzyme expression were associated with changes in liver health. There was a significant group effect on particle diameter as a marker of hepatic lipid deposition. Mean particle diameter was greater in OLETF compared with LETO, and ARB treatment had no effect (Fig. 11, *A* and *B*). There were no detectable differences in fibrosis and necrosis among the groups at this stage.

DISCUSSION

Obesity predisposes individuals to the development of cardiovascular and metabolic disorders (34, 35). Notably, some hypertension treatments are associated with the development or worsening of hyperglycemia (36, 37). Nevertheless, a meta-analysis found that RAS inhibitors delay the new onset of T2D in hypertensive or individuals with a high risk for cardiovascular disease (38). Furthermore, in rodent models of obesity and insulin resistance, RAS blockade's benefits on dysglycemia seem to be isolated to improvements in insulin signaling in skeletal muscle, adipose, and liver (17, 25, 39–41). Nevertheless, these tissues' dynamic cellular responses that may contribute to the beneficial effects of chronic AT_1 blockade on glucose intolerance are not well-defined. Therefore, we aimed to evaluate the static and dynamic responses of soleus muscle, liver, and adipose to an acute glucose challenge following the chronic blockade of AT_1. This study demonstrates that chronic AT_1 blockade in OLETF rats *1*) decreases adipocyte inflammation and *2*) increases GLUT4 protein expression in retroperitoneal fat. Additionally, chronic AT_1 blockade *3*) increases IR phosphorylation in retroperitoneal fat and *4*) decreases the expression of genes involved in hepatic gluconeogenesis after an acute glucose challenge. Collectively, these results suggest that the overactivation of RAS associated with the manifestation glucose intolerance in OLETF rats contributes to the development of hyperglycemia by increasing the adipocyte inflammatory response and by decreasing IR phosphorylation in adipose while also increasing hepatic glucose production.

Insulin suppresses hepatic glucose production directly by decreasing the expression of genes involved in hepatic glucose production (42). Nevertheless, insulin can still regulate hepatic glucose production in mice that lack components of hepatic insulin signaling and *Foxo1* (43, 44) suggesting that insulin can regulate hepatic gluconeogenesis through its actions on other tissues. In the present study, acute glucose exposure had no effect on hepatic IR phosphorylation and AKT phosphorylation in OLETF and chronic AT_1 blockade had no profound effects in this regard. However, AT_1 blockade decreased hepatic *Pck1* and *G6pc1* mRNA expressions suggesting that RAS inhibition may decrease hepatic gluconeogenesis independent of its effects on hepatic IR

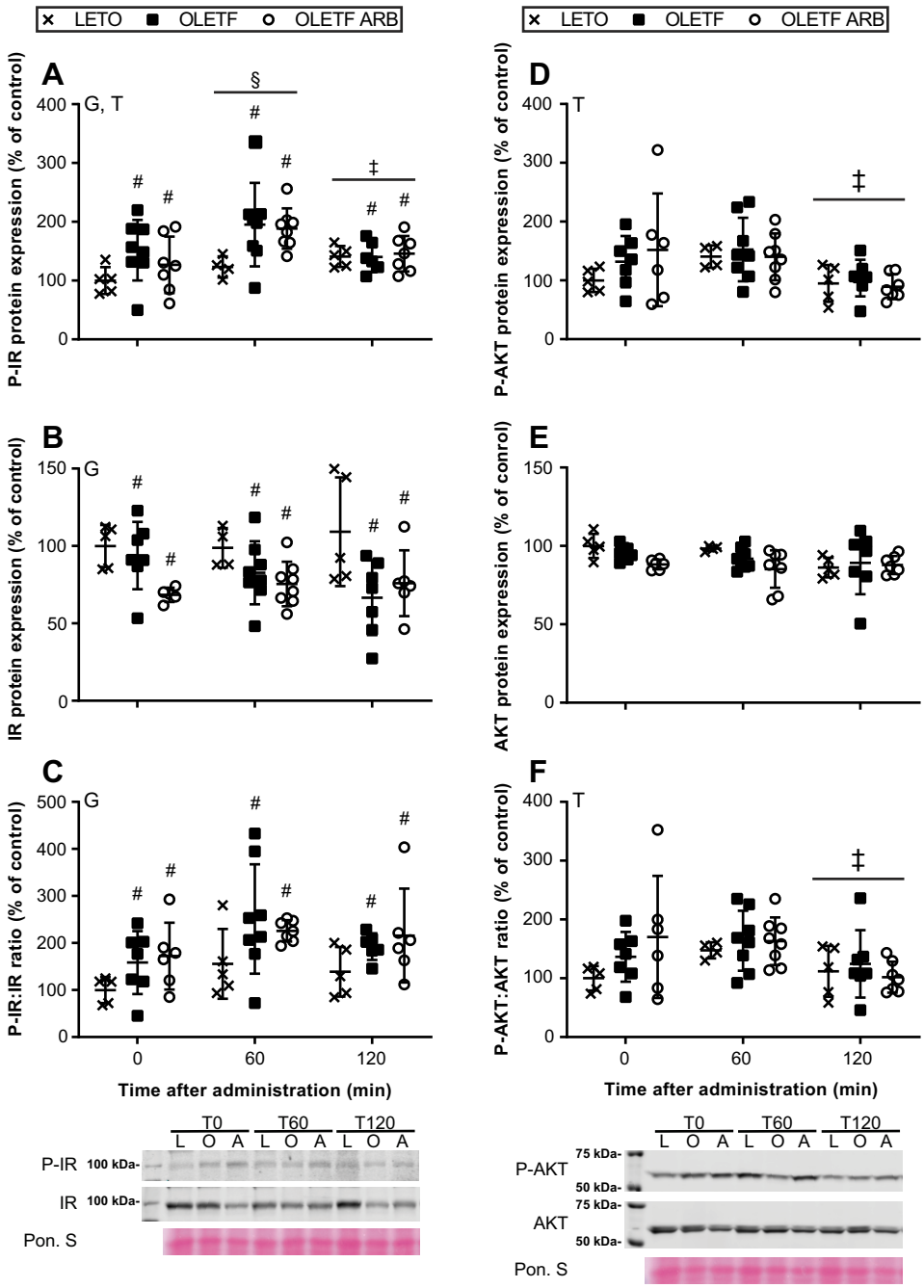

Figure 9. IR phosphorylation and AKT phosphorylation are not impaired in liver of Otsuka Long-Evans Tokushima Fatty (OLETF) rats. Means (±SD) IR phosphorylation (*A*), IR-β (*B*), p-IR:IR-β ratio (*C*), AKT phosphorylation (*D*), AKT (*E*), and p-AKT:AKT ratio (*F*) [% change from Long-Evans Tokushima Otsuka (LETO) *T0*] and their representative Western blot bands in LETO (n = 4 or 5/time point), OLETF (n = 6–8/time point), and OLETF + ARB (n = 6–8/time point) prior (*T0*) and 60 (*T60*) and 120 (*T120*) min after challenge of glucose. Comparisons were assessed using a mixed-model ANOVA with group and time as between-subject factors. Multiple comparisons were carried out using a Holm–Sidak correction. G = group $P < 0.05$; T = time $P < 0.05$. #$P < 0.05$ vs. LETO; §$P < 0.05$ vs. *T0*; ‡$P < 0.05$ vs. *T60*. ARB, angiotensin receptor type 1 (AT_1) blocker; IR, insulin receptor.

phosphorylation and AKT phosphorylation. In streptozotocin-induced type 1 diabetic rats, AT_1 inhibition decreased hepatic phosphoenolpyruvate carboxykinase protein (21). Obesity is associated with increased hypothalamic-pituitary-adrenal (HPA) axis activity (45). In obese Zucker rats, chronic ANG II treatment increases the pituitary-adrenal response to a corticotropin-releasing hormone (CRH) challenge (46), and in spontaneously hypertensive rats, both AT_1 and angiotensin-converting enzyme inhibition decreased the pituitary-adrenal response to a CRH challenge (47). In the latter study, spontaneously hypertensive rats treated with candesartan also had lower plasma glucose and higher plasma insulin in response to the CRH challenge (47). Additionally, we previously showed that chronic AT_1 inhibition decreased corticosterone in OLETF rats (48). In the present study, we found glucose suppressed corticosterone levels only at the 120-min time point in the ARB group suggesting that chronic inhibition of AT_1 does not likely alter the expression of gluconeogenic genes statically via corticosterone but may do so dynamically in response to a glucose load. Therefore, we hypothesize that ANG II may act directly in the nucleus to regulate gene expression as ANG II is increased in hepatic nuclei and increased RNA transcription (49, 50). ANG II may also regulate the activity of gluconeogenic enzymes as intravenous infusion of ANG II increased hepatic glucose production within 10 min (51–53). However, these hypotheses need

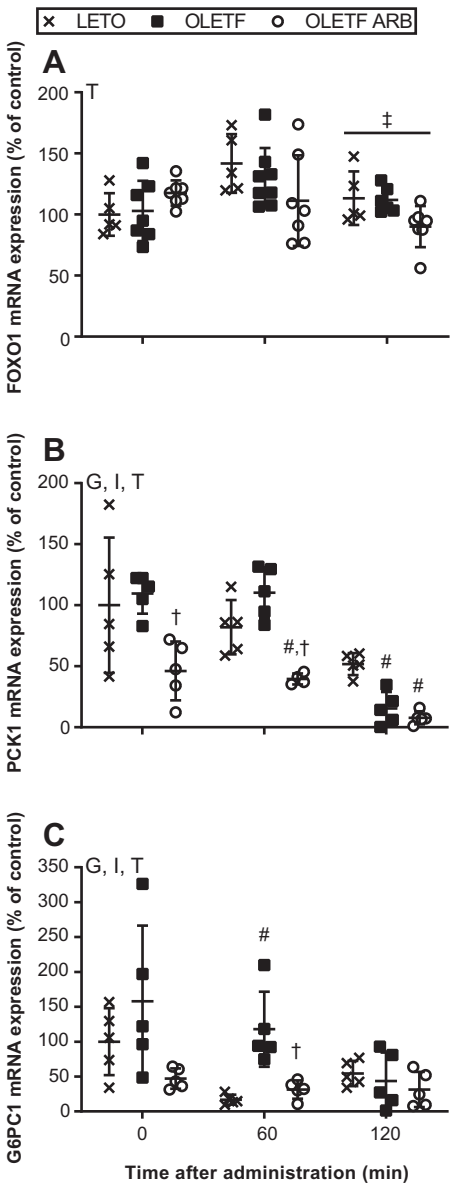

Figure 10. AT_1 blockade reduces the expression of genes involved in hepatic gluconeogenesis. Means (±SD) Forkhead Box O1 (FOXO1; *A*), phosphoenolpyruvate carboxykinase 1 (PCK1; *B*), and glucose-6-phosphatase 1 (G6PC1; *C*) mRNA expression [% change from Long-Evans Tokushima Otsuka (LETO) *T0*] of LETO (n = 4 or 5/time point), Otsuka Long-Evans Tokushima Fatty (OLETF; n = 5–8/time point), and OLETF + ARB (n = 5–8/time point) prior (*T0*) and 60 (*T60*) and 120 (*T120*) min after challenge of glucose. Comparisons were assessed using a mixed-model ANOVA with group and time as between-subject factors. Multiple comparisons were carried out using a Holm–Sidak correction. G = group $P < 0.05$; I = interaction $P < 0.05$; T = time $P < 0.05$. #$P < 0.05$ vs. LETO; †$P < 0.05$ vs. OLETF. ARB, angiotensin receptor type 1 (AT_1) blocker. ‡$P < 0.05$ vs. T60.

to be tested to determine the mechanism by which AT_1 inhibition decreases hepatic glucose production, especially in relation to changes in glucocorticoids.

Skeletal muscle accounts for the majority of postprandial glucose disposal (54). Notably, the deletion of the IR in skeletal muscle decreases insulin-stimulated glucose uptake in muscle. However, the IR null mice do not develop hyperglycemia or glucose intolerance due to other tissues, such as adipose, compensating for this defect (55). In contrast, the deletion of the IR in adipose leads to lipodystrophy, systemic insulin resistance, and the development of nonalcoholic fatty liver disease (NAFLD) that progresses to nonalcoholic steatohepatitis (NASH) (56, 57). Disruption of insulin signaling in adipose without deleting the IR, by knocking out the target of rapamycin complex 2, decreases glucose uptake, lipogenesis, and increases inflammation in adipose while also increasing hepatic glucose production (58, 59). Furthermore, mice with deletion of the phosphatase and tensin homolog (PTEN) in adipocytes are characterized by enhanced insulin signaling in adipose and increased fat mass. However, these mice have decreased inflammation and do not develop fasting hyperglycemia, glucose intolerance, or NAFLD in response to a high-fat diet (60). These studies suggest that disruption of insulin signaling in adipose reduces glucose uptake, lipogenesis, increases inflammation, and lipolysis in adipose resulting in systemic insulin resistance and ectopic lipid deposition in peripheral tissues. In the present study, we demonstrated that chronic AT_1 inhibition increased IR phosphorylation in response to acute glucose exposure and decreased TNF-α expression and macrophage infiltration in adipose. In addition, we previously showed in age-matched OLETF rats that treatment with etanercept, a TNF-α inhibitor, improved glucose tolerance to greater levels than AT_1 inhibition and cotreatment did not have an additive effect (29). Although chronic AT_1 inhibition increased IR phosphorylation after an acute glucose exposure, this effect did not translate into increased AKT phosphorylation. The lack of an increase in AKT phosphorylation may result from measuring its phosphorylation at the whole cell level instead of that bound to the plasma membrane, which was shown in 3T3-L1

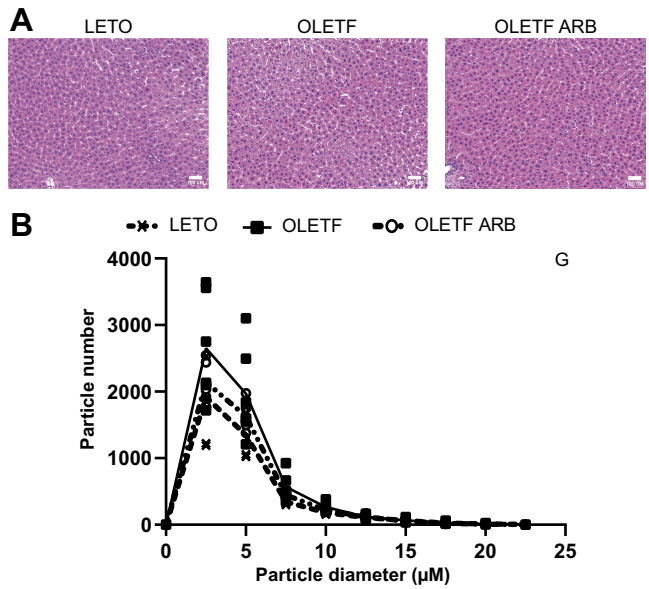

Figure 11. Effects of chronic AT_1 blockade on hepatic lipid deposition. *A*: representative images of H&E-stained livers. Means (±SD) particle diameter distribution (*B*) of Long-Evans Tokushima Otsuka (LETO; n = 5), Otsuka Long-Evans Tokushima Fatty (OLETF; n = 6), and OLETF + ARB (n = 5). Comparisons were assessed using a mixed-model ANOVA with group as between-subjects factor and particle diameter as a within-subjects factor. G = group $P < 0.05$; I = interaction $P < 0.05$. ARB, angiotensin receptor type 1 (AT_1) blocker.

adipocytes to determine its activity (61). Nevertheless, chronic AT_1 blockade increased GLUT4 protein levels suggesting that AKT activity was likely increased at some point that was not captured in our measurement periods here. Collectively, our results suggest that at this early stage of the disease, inappropriately activated RAS may increase the adipocyte inflammatory response leading to decreased IR phosphorylation and GLUT4 expression that ultimately contribute to the development of hyperglycemia.

We previously demonstrated that chronic AT_1 blockade decreased the abundance of large adipocytes and that this improvement in adipocyte morphology was associated with an improvement in the ability to suppress NEFA levels (lipolysis) after an acute glucose challenge in OLETF rats (10). In the present study, chronic AT_1 blockade had minor effects on adipocyte morphology and did not affect plasma NEFA levels postglucose challenge at the measurement time points. The discrepancies between these two studies may result from the animals being younger in the present study (16 wk compared with 24 wk) and less insulin-resistant. Other tissues such as the liver may compensate and sequester the excess free fatty acids released from lipolysis at this stage of the condition. Indeed, at this stage of the disease, OLETF rats have greater lipid deposition as demonstrated by particle analysis in the present study and greater hepatic triglycerides in our previous study (48). Collectively, these results suggest that at this stage of the disease, peripheral tissues such as the liver sequester free fatty acids at a rate that surpasses that of lipolysis; however, as the condition progresses, the capacity of peripheral tissues to compensate for the increase in lipolysis leading to a sustained elevation in free fatty acids following the acute glucose challenge is diminished.

Conclusions

In summary, the present study demonstrated that chronic activation of AT_1 worsened glucose tolerance by increasing adipocyte inflammation and impairing adipose IR phosphorylation and GLUT4 expression and by increasing the expression of genes involved in hepatic gluconeogenesis, likely resulting in elevated hepatic glucose production. Thus, the early onset of hyperglycemia is characterized by impaired IR phosphorylation in adipose following an acute glucose challenge (or postprandial event) that is, at least partially, AT_1-mediated. In adipose, the impaired IR phosphorylation coincides with increased adipocyte inflammation and our results suggest that adipocyte inflammation may precede the impairment in adipocyte IR phosphorylation.

ACKNOWLEDGMENTS

We thank Dr. K. Kitada, Dr. K. Islam, Dr. M. Thorwald, M Seki, Dr. M. Cornejo, and Dr. D. Gravano for their assistance during dissections and with laboratory analyses. We thank H. Aaron and F. Ives for their microscopy training and N. Reyes for assistance with staining. We thank Dr. J. Dhillon for assistance with the statistical analysis. Finally, we are grateful to Drs. N. Oviedo, F. Wolf, and S.H. Adams for their discussion of the results and helpful comments on the manuscript. Olmesartan was kindly donated by Daiichi-Sankyo (Tokyo, Japan) to Dr. A. Nishiyama.

GRANTS

R. Rodriguez was supported by NIH National Institute on Minority Health and Health Disparities (NIMHD) 9T37MD001480 and National Institute of General Medical Science K12GM081266, US Department of Agriculture HSI Educational Grant 2017–03691 and by a Faculty Mentor Program Fellowship from the University of California, Merced Graduate Division. A.Y. Lee and B. Martinez were supported by NIH NIMHD 9T37MD001480. R.M. Ortiz was partially supported by NIH National Heart, Lung, and Blood Institute (NHLBI) K02HL103787. Research was partially funded by NIH NHLBI R01HL091767.

DISCLOSURES

No conflicts of interest, financial or otherwise, are declared by the authors.

AUTHOR CONTRIBUTIONS

R.R., D.N., A.N., and R.M.O. conceived and designed research; R.R., A.Y.L., J.A.G-L., B.M., H.O., and J.P.V-M. performed experiments; R.R., H.O., and J.P.V-M. analyzed data; R.R., H.O., and R.M.O. interpreted results of experiments; R.R. and J.P.V-M. prepared figures; R.R. and J.P.V-M. drafted manuscript; R.R., A.Y.L., J.A.G-L., B.M., D.N., D.G.P., A.N., J.P.V-M., and R.M.O. edited and revised manuscript; R.R., A.Y.L., J.A.G-L., B.M., D.N., D.G.P., A.N., H.O., J.P.V-M., and R.M.O. approved final version of manuscript.

REFERENCES

1. **Saltiel AR**, **Kahn CR.** Insulin signalling and the regulation of glucose and lipid metabolism. *Nature* 414: 799–806, 2001. doi:10.1038/414799a.
2. **Weyer C**, **Bogardus C**, **Mott DM**, **Pratley RE.** The natural history of insulin secretory dysfunction and insulin resistance in the pathogenesis of type 2 diabetes mellitus. *J Clin Invest* 104: 787–794, 1999. doi:10.1172/JCI7231.
3. **Bonadonna RC**, **Groop L**, **Kraemer N**, **Ferrannini E**, **Del Prato S**, **DeFronzo RA.** Obesity and insulin resistance in humans: a dose-response study. *Metabolism* 39: 452–459, 1990. doi:10.1016/0026-0495(90)90002-t.
4. **Guilherme A**, **Virbasius JV**, **Puri V**, **Czech MP.** Adipocyte dysfunctions linking obesity to insulin resistance and type 2 diabetes. *Nat Rev Mol Cell Biol* 9: 367–377, 2008. doi:10.1038/nrm2391.
5. **Kahn BB**, **Flier JS.** Obesity and insulin resistance. *J Clin Invest* 106: 473–481, 2000. doi:10.1172/JCI10842.
6. **Heilbronn LK**, **Campbell LV.** Adipose tissue macrophages, low grade inflammation and insulin resistance in human obesity. *Curr Pharm Des* 14: 1225–1230, 2008. doi:10.2174/138161208784246153.
7. **Engeli S**, **Böhnke J**, **Gorzelniak K**, **Janke J**, **Schling P**, **Bader M**, **Luft FC**, **Sharma AM.** Weight loss and the renin-angiotensin-aldosterone system. *Hypertension* 45: 356–362, 2005. doi:10.1161/01.HYP.0000154361.47683.d3.
8. **Boustany CM**, **Bharadwaj K**, **Daugherty A**, **Brown DR**, **Randall DC**, **Cassis LA.** Activation of the systemic and adipose renin-angiotensin system in rats with diet-induced obesity and hypertension. *Am J Physiol Regul Integr Comp Physiol* 287: R943–R949, 2004. doi:10.1152/ajpregu.00265.2004.
9. **Lau T**, **Carlsson PO**, **Leung PS.** Evidence for a local angiotensin-generating system and dose-dependent inhibition of glucose-stimulated insulin release by angiotensin II in isolated pancreatic islets. *Diabetologia* 47: 240–248, 2004. doi:10.1007/s00125-003-1295-1.
10. **Rodriguez R**, **Minas JN**, **Vazquez-Medina JP**, **Nakano D**, **Parkes DG**, **Nishiyama A**, **Ortiz RM.** Chronic AT1 blockade improves glucose homeostasis in obese OLETF rats. *J Endocrinol* 237: 271–284, 2018. doi:10.1530/JOE-17-0678.
11. **Rodriguez R**, **Viscarra JA**, **Minas JN**, **Nakano D**, **Nishiyama A**, **Ortiz RM.** Angiotensin receptor blockade increases pancreatic insulin secretion and decreases glucose intolerance during glucose

supplementation in a model of metabolic syndrome. *Endocrinology* 153: 1684–1695, 2012. doi:10.1210/en.2011-1885.

12. **Benson SC**, **Pershadsingh HA**, **Ho CI**, **Chittiboyina A**, **Desai P**, **Pravenec M**, **Qi N**, **Wang J**, **Avery MA**, **Kurtz TW.** Identification of telmisartan as a unique angiotensin II receptor antagonist with selective PPARgamma-modulating activity. *Hypertension* 43: 993–1002, 2004. doi:10.1161/01.HYP.0000123072.34629.57.
13. **Miesel A**, **Müller-Fielitz H**, **Jöhren O**, **Vogt FM**, **Raasch W.** Double blockade of angiotensin II (AT(1))—receptors and ACE does not improve weight gain and glucose homeostasis better than single-drug treatments in obese rats. *Br J Pharmacol* 165: 2721–2735, 2012. doi:10.1111/j.1476-5381.2011.01726.x.
14. **Müller-Fielitz H**, **Hübel N**, **Mildner M**, **Vogt FM**, **Barkhausen J**, **Raasch W.** Chronic blockade of angiotensin AT(1) receptors improves cardinal symptoms of metabolic syndrome in diet-induced obesity in rats. *Br J Pharmacol* 171: 746–760, 2014. doi:10.1111/bph.12510.
15. **Müller-Fielitz H**, **Landolt J**, **Heidbreder M**, **Werth S**, **Vogt FM**, **Jöhren O**, **Raasch W.** Improved insulin sensitivity after long-term treatment with AT1 blockers is not associated with PPARγ target gene regulation. *Endocrinology* 153: 1103–1115, 2012. doi:10.1210/en.2011-0183.
16. **Nagai Y**, **Ichihara A**, **Nakano D**, **Kimura S**, **Pelisch N**, **Fujisawa Y**, **Hitomi H**, **Hosomi N**, **Kiyomoto H**, **Kohno M**, **Ito H**, **Nishiyama A.** Possible contribution of the non-proteolytic activation of prorenin to the development of insulin resistance in fructose-fed rats. *Exp Physiol* 94: 1016–1023, 2009. doi:10.1113/expphysiol.2009.048108.
17. **Muñoz MC**, **Giani JF**, **Dominici FP**, **Turyn D**, **Toblli JE.** Long-term treatment with an angiotensin II receptor blocker decreases adipocyte size and improves insulin signaling in obese Zucker rats. *J Hypertens* 27: 2409–2420, 2009. doi:10.1097/HJH.0b013e3283310e1b.
18. **Fujisaka S**, **Usui I**, **Kanatani Y**, **Ikutani M**, **Takasaki I**, **Tsuneyama K**, **Tabuchi Y**, **Bukhari A**, **Yamazaki Y**, **Suzuki H**, **Senda S**, **Aminuddin A**, **Nagai Y**, **Takatsu K**, **Kobayashi M**, **Tobe K.** Telmisartan improves insulin resistance and modulates adipose tissue macrophage polarization in high-fat-fed mice. *Endocrinology* 152: 1789–1799, 2011. doi:10.1210/en.2010-1312.
19. **Henriksen EJ**, **Jacob S**, **Kinnick TR**, **Teachey MK**, **Krekler M.** Selective angiotensin II receptor antagonism reduces insulin resistance in obese Zucker rats. *Hypertension* 38: 884–890, 2001. doi:10.1161/hy1101.092970.
20. **Shiuchi T**, **Iwai M**, **Li HS**, **Wu L**, **Min LJ**, **Li JM**, **Okumura M**, **Cui TX**, **Horiuchi M.** Angiotensin II type-1 receptor blocker valsartan enhances insulin sensitivity in skeletal muscles of diabetic mice. *Hypertension* 43: 1003–1010, 2004. doi:10.1161/01.HYP.0000125142.41703.64.
21. **Chan P**, **Wong KL**, **Liu IM**, **Tzeng TF**, **Yang TL**, **Cheng JT.** Antihyperglycemic action of angiotensin II receptor antagonist, valsartan, in streptozotocin-induced diabetic rats. *J Hypertens* 21: 761–769, 2003. doi:10.1097/00004872-200304000-00020.
22. **Ran J**, **Hirano T**, **Adachi M.** Angiotensin II type 1 receptor blocker ameliorates overproduction and accumulation of triglyceride in the liver of Zucker fatty rats. *Am J Physiol Endocrinol Metab* 287: E227–E232, 2004. doi:10.1152/ajpendo.00090.2004.
23. **Henriksen EJ**, **Prasannarong M.** The role of the renin-angiotensin system in the development of insulin resistance in skeletal muscle. *Mol Cell Endocrinol* 378: 15–22, 2013. doi:10.1016/j.mce.2012.04.011.
24. **Iwai M**, **Li HS**, **Chen R**, **Shiuchi T**, **Wu L**, **Min LJ**, **Li JM**, **Tsuda M**, **Suzuki J**, **Tomono Y**, **Tomochika H**, **Mogi M**, **Horiuchi M.** Calcium channel blocker azelnidipine reduces glucose intolerance in diabetic mice via different mechanism than angiotensin receptor blocker olmesartan. *J Pharmacol Exp Ther* 319: 1081–1087, 2006. doi:10.1124/jpet.106.108894.
25. **Muñoz MC**, **Argentino DP**, **Dominici FP**, **Turyn D**, **Toblli JE.** Irbesartan restores the in-vivo insulin signaling pathway leading to Akt activation in obese Zucker rats. *J Hypertens* 24: 1607–1617, 2006. doi:10.1097/01.hjh.0000239297.63377.3f.
26. **Kawano K**, **Hirashima T**, **Mori S**, **Natori T.** OLETF (Otsuka Long-Evans Tokushima Fatty) rat: a new NIDDM rat strain. *Diabetes Res Clin Pract* 24 Suppl: S317–S320, 1994. doi:10.1016/0168-8227(94)90269-0.
27. **Kawano K**, **Hirashima T**, **Mori S**, **Saitoh Y**, **Kurosumi M**, **Natori T.** Spontaneous long-term hyperglycemic rat with diabetic complications. Otsuka Long-Evans Tokushima Fatty (OLETF) strain. *Diabetes* 41: 1422–1428, 1992. doi:10.2337/diab.41.11.1422.
28. **Thorwald M**, **Rodriguez R**, **Lee A**, **Martinez B**, **Peti-Peterdi J**, **Nakano D**, **Nishiyama A**, **Ortiz RM.** Angiotensin receptor blockade improves cardiac mitochondrial activity in response to an acute glucose load in obese insulin resistant rats. *Redox Biol* 14: 371–378, 2018. doi:10.1016/j.redox.2017.10.005.
29. **Rodriguez R**, **Lee A**, **Mathis KW**, **Broome HJ**, **Thorwald M**, **Martinez B**, **Nakano D**, **Nishiyama A**, **Ryan MJ**, **Ortiz RM.** Angiotensin receptor and tumor necrosis factor-α activation contributes to glucose intolerance independent of systolic blood pressure in obese rats. *Am J Physiol Renal Physiol* 315: F1081–F1090, 2018. doi:10.1152/ajprenal.00156.2018.
30. **Erbe DV**, **Gartrell K**, **Zhang Y-L**, **Suri V**, **Kirincich SJ**, **Will S**, **Perreault M**, **Wang S**, **Tobin JF.** Molecular activation of PPARγ by angiotensin II type 1-receptor antagonists. *Vasc Pharmacol* 45: 154–162, 2006. doi:10.1016/j.vph.2006.05.002.
31. **Piao D**, **Ritchey JW**, **Holyoak GR**, **Wall CR**, **Sultana N**, **Murray JK**, **Bartels KE.** In vivo percutaneous reflectance spectroscopy of fatty liver development in rats suggests that the elevation of the scattering power is an early indicator of hepatic steatosis. *J Innov Opt Health Sci* 11: 1850019, 2018. doi:10.1142/S1793545818500190.
32. **Vázquez-Medina JP**, **Dodia C**, **Weng L**, **Mesaros C**, **Blair IA**, **Feinstein SI**, **Chatterjee S**, **Fisher AB.** The phospholipase A2 activity of peroxiredoxin 6 modulates NADPH oxidase 2 activation via lysophosphatidic acid receptor signaling in the pulmonary endothelium and alveolar macrophages. *FASEB J* 30: 2885–2898, 2016. doi:10.1096/fj.201500146R.
33. **Morgan-Bathke M**, **Harteneck D**, **Jaeger P**, **Sondergaard E**, **Karwoski R**, **Espinosa De Ycaza A**, **Carranza-Leon BG**, **Faubion WA Jr**, **Oliveira AM**, **Jensen MD.** Comparison of methods for analyzing human adipose tissue macrophage content. *Obesity (Silver Spring)* 25: 2100–2107, 2017. doi:10.1002/oby.22012.
34. **Nguyen NT**, **Magno CP**, **Lane KT**, **Hinojosa MW**, **Lane JS.** Association of hypertension, diabetes, dyslipidemia, and metabolic syndrome with obesity: findings from the National Health and Nutrition Examination Survey, 1999 to 2004. *J Am Coll Surg* 207: 928–934, 2008. doi:10.1016/j.jamcollsurg.2008.08.022.
35. **Willett WC**, **Dietz WH**, **Colditz GA.** Guidelines for healthy weight. *N Engl J Med* 341: 427–434, 1999. doi:10.1056/NEJM199908053410607.
36. **Gress TW**, **Nieto FJ**, **Shahar E**, **Wofford MR**, **Brancati FL.** Hypertension and antihypertensive therapy as risk factors for type 2 diabetes mellitus. Atherosclerosis Risk in Communities Study. *N Engl J Med* 342: 905–912, 2000. doi:10.1056/NEJM200003303421301.
37. **Eriksson JW**, **Jansson P-A**, **Carlberg B**, **HäGg A**, **Kurland L**, **Svensson MK**, **AhlströM HKAN**, **StröM C**, **LöNn L**, **ÖJbrandt K**, **Johansson L**, **Lind L.** Hydrochlorothiazide, but not Candesartan, aggravates insulin resistance and causes visceral and hepatic fat accumulation: the mechanisms for the diabetes preventing effect of Candesartan (MEDICA) Study. *Hypertension* 52: 1030–1037, 2008. doi:10.1161/HYPERTENSIONAHA.108.119404.
38. **Tocci G**, **Paneni F**, **Palano F**, **Sciarretta S**, **Ferrucci A**, **Kurtz T**, **Mancia G**, **Volpe M.** Angiotensin-converting enzyme inhibitors, angiotensin II receptor blockers and diabetes: a meta-analysis of placebo-controlled clinical trials. *Am J Hypertens* 24: 582–590, 2011. doi:10.1038/ajh.2011.8.
39. **Lastra G**, **Habibi J**, **Whaley-Connell AT**, **Manrique C**, **Hayden MR**, **Rehmer J**, **Patel K**, **Ferrario C**, **Sowers JR.** Direct renin inhibition improves systemic insulin resistance and skeletal muscle glucose transport in a transgenic rodent model of tissue renin overexpression. *Endocrinology* 150: 2561–2568, 2009. doi:10.1210/en.2008-1391.
40. **Sloniger JA**, **Saengsirisuwan V**, **Diehl CJ**, **Kim JS**, **Henriksen EJ.** Selective angiotensin II receptor antagonism enhances whole-body insulin sensitivity and muscle glucose transport in hypertensive TG (mREN2)27 rats. *Metabolism* 54: 1659–1668, 2005. doi:10.1016/j.metabol.2005.06.016.
41. **Marchionne EM**, **Diamond-Stanic MK**, **Prasonnarong M**, **Henriksen EJ.** Chronic renin inhibition with aliskiren improves glucose tolerance, insulin sensitivity, and skeletal muscle glucose transport activity in obese Zucker rats. *Am J Physiol Regul Integr Comp Physiol* 302: R137–R142, 2012. doi:10.1152/ajpregu.00448.2011.
42. **Li X**, **Monks B**, **Ge Q**, **Birnbaum MJ.** Akt/PKB regulates hepatic metabolism by directly inhibiting PGC-1α transcription coactivator. *Nature* 447: 1012–1016, 2007. doi:10.1038/nature05861.

43. **Titchenell PM**, **Chu Q**, **Monks BR**, **Birnbaum MJ.** Hepatic insulin signalling is dispensable for suppression of glucose output by insulin in vivo. *Nat Commun* 6: 7078, 2015. doi:10.1038/ncomms8078.
44. **Lu M**, **Wan M**, **Leavens KF**, **Chu Q**, **Monks BR**, **Fernandez S**, **Ahima RS**, **Ueki K**, **Kahn CR**, **Birnbaum MJ.** Insulin regulates liver metabolism in vivo in the absence of hepatic Akt and Foxo1. *Nat Med* 18: 388–395, 2012. doi:10.1038/nm.2686.
45. **Pasquali R**, **Vicennati V**, **Cacciari M**, **Pagotto U.** The hypothalamic-pituitary-adrenal axis activity in obesity and the metabolic syndrome. *Ann NY Acad Sci* 1083: 111–128, 2006. doi:10.1196/annals.1367.009.
46. **Müller H**, **Schweitzer N**, **Jöhren O**, **Dominiak P**, **Raasch W.** Angiotensin II stimulates the reactivity of the pituitary-adrenal axis in leptin-resistant Zucker rats, thereby influencing the glucose utilization. *Am J Physiol Endocrinol Metab* 293: E802–E810, 2007. doi:10.1152/ajpendo.00650.2006.
47. **Raasch W**, **Wittmershaus C**, **Dendorfer A**, **Voges I**, **Pahlke F**, **Dodt C**, **Dominiak P**, **JöHren O.** Angiotensin II inhibition reduces stress sensitivity of hypothalamo-pituitary-adrenal axis in spontaneously hypertensive rats. *Endocrinology* 147: 3539–3546, 2006. doi:10.1210/en.2006-0198.
48. **Montez P**, **Vázquez-Medina JP**, **Rodríguez R**, **Thorwald MA**, **Viscarra JA**, **Lam L**, **Peti-Peterdi J**, **Nakano D**, **Nishiyama A**, **Ortiz RM.** Angiotensin receptor blockade recovers hepatic UCP2 expression and aconitase and SDH activities and ameliorates hepatic oxidative damage in insulin resistant rats. *Endocrinology* 153: 5746–5759, 2012. doi:10.1210/en.2012-1390.
49. **Booz GW**, **Conrad KM**, **Hess AL**, **Singer HA**, **Baker KM.** Angiotensin-II-binding sites on hepatocyte nuclei. *Endocrinology* 130: 3641–3649, 1992. doi:10.1210/endo.130.6.1597161.
50. **Eggena P**, **Zhu JH**, **Clegg K**, **Barrett JD.** Nuclear angiotensin receptors induce transcription of renin and angiotensinogen mRNA. *Hypertension* 22: 496–501, 1993. doi:10.1161/01.hyp.22.4.496.
51. **Coimbra CC**, **Garofalo MAR**, **Foscolo DRC**, **Xavier AR**, **Migliorini RH.** Gluconeogenesis activation after intravenous angiotensin II in freely moving rats. *Peptides* 20: 823–827, 1999. doi:10.1016/S0196-9781(99)00068-6.
52. **Machado L**, **Marubayashi U**, **Reis A**, **Coimbra C.** The hyperglycemia induced by angiotensin II in rats is mediated by AT1 receptors. *Braz J Med Biol Res* 31: 1349–1352, 1998. doi:10.1590/S0100-879X1998001000018.
53. **Reisenleiter F**, **Katz N**, **Gardemann A.** Control of hepatic carbohydrate metabolism and haemodynamics in perfused rat liver by arterial and portal angiotensin II. *Eur J Gastroenterol Hepatol* 8: 279–286, 1996. doi:10.1097/00042737-199603000-00017.
54. **DeFronzo RA.** Lilly lecture 1987. The triumvirate: beta-cell, muscle, liver. A collusion responsible for NIDDM. *Diabetes* 37: 667–687, 1988. doi:10.2337/diab.37.6.667.
55. **Brüning JC**, **Michael MD**, **Winnay JN**, **Hayashi T**, **Hörsch D**, **Accili D**, **Goodyear LJ**, **Kahn CR.** A muscle-specific insulin receptor knockout exhibits features of the metabolic syndrome of NIDDM without altering glucose tolerance. *Mol Cell* 2: 559–569, 1998. doi:10.1016/s1097-2765(00)80155-0.
56. **Boucher J**, **Softic S**, **El Ouaamari A**, **Krumpoch MT**, **Kleinridders A**, **Kulkarni RN**, **O'Neill BT**, **Kahn CR.** Differential roles of insulin and IGF-1 receptors in adipose tissue development and function. *Diabetes* 65: 2201–2213, 2016. doi:10.2337/db16-0212.
57. **Softic S**, **Boucher J**, **Solheim MH**, **Fujisaka S**, **Haering MF**, **Homan EP**, **Winnay J**, **Perez-Atayde AR**, **Kahn CR.** Lipodystrophy due to adipose tissue-specific insulin receptor knockout results in progressive NAFLD. *Diabetes* 65: 2187–2200, 2016. doi:10.2337/db16-0213.
58. **Tang Y**, **Wallace M**, **Sanchez-Gurmaches J**, **Hsiao WY**, **Li H**, **Lee PL**, **Vernia S**, **Metallo CM**, **Guertin DA.** Adipose tissue mTORC2 regulates ChREBP-driven de novo lipogenesis and hepatic glucose metabolism. *Nat Commun* 7: 11365, 2016. doi:10.1038/ncomms11365.
59. **Shimobayashi M**, **Albert V**, **Woelnerhanssen B**, **Frei IC**, **Weissenberger D**, **Meyer-Gerspach AC**, **Clement N**, **Moes S**, **Colombi M**, **Meier JA**, **Swierczynska MM**, **Jenö P**, **Beglinger C**, **Peterli R**, **Hall MN.** Insulin resistance causes inflammation in adipose tissue. *J Clin Invest* 128: 1538–1550, 2018. doi:10.1172/JCI96139.
60. **Morley TS**, **Xia JY**, **Scherer PE.** Selective enhancement of insulin sensitivity in the mature adipocyte is sufficient for systemic metabolic improvements. *Nat Commun* 6: 7906, 2015. doi:10.1038/ncomms8906.
61. **Gonzalez E**, **McGraw TE.** Insulin-modulated Akt subcellular localization determines Akt isoform-specific signaling. *Proc Natl Acad Sci USA* 106: 7004–7009, 2009. doi:10.1073/pnas.0901933106.